The structure of an *E. coli* $tRNA_f^{Met}$ A_1–U_{72} variant shows an unusual conformation of the A_1–U_{72} base pair

AURIANE MONESTIER, ALEXEY ALEKSANDROV,[1] PIERRE-DAMIEN COUREUX,[1] MICHEL PANVERT, YVES MECHULAM, and EMMANUELLE SCHMITT

Laboratoire de Biochimie, Ecole polytechnique, CNRS, Université Paris-Saclay, 91128 Palaiseau cedex, France

ABSTRACT

Translation initiation in eukaryotes and archaea involves a methionylated initiator tRNA delivered to the ribosome in a ternary complex with e/aIF2 and GTP. Eukaryotic and archaeal initiator tRNAs contain a highly conserved A_1–U_{72} base pair at the top of the acceptor stem. The importance of this base pair to discriminate initiator tRNAs from elongator tRNAs has been established previously using genetics and biochemistry. However, no structural data illustrating how the A_1–U_{72} base pair participates in the accurate selection of the initiator tRNAs by the translation initiation systems are available. Here, we describe the crystal structure of a mutant *E. coli* initiator $tRNA_f^{Met}A_1$–U_{72}, aminoacylated with methionine, in which the C_1:A_{72} mismatch at the end of the tRNA acceptor stem has been changed to an A_1–U_{72} base pair. Sequence alignments show that the mutant *E. coli* tRNA is a good mimic of archaeal initiator tRNAs. The crystal structure, determined at 2.8 Å resolution, shows that the A_1–U_{72} pair adopts an unusual arrangement. A_1 is in a *syn* conformation and forms a single H-bond interaction with U_{72}. This interaction requires protonation of the N1 atom of A_1. Moreover, the 5′ phosphoryl group folds back into the major groove of the acceptor stem and interacts with the N7 atom of G_2. A possible role of this unusual geometry of the A_1–U_{72} pair in the recognition of the initiator tRNA by its partners during eukaryotic and archaeal translation initiation is discussed.

Keywords: X-ray crystallography; tRNA; translation initiation

INTRODUCTION

The initiator $tRNA_i^{Met}$ (called $tRNA_f^{Met}$ in bacteria and organelles) plays a central role in decoding mRNA into proteins. Its recruitment by the translation initiation machinery allows setting of the reading frame of the mRNA by decoding the correct initiation codon. Selection of the initiator tRNA by the translation initiation machinery and its rejection by the elongation system involve some nucleotidic sequence features that distinguish it from elongator tRNAs, in particular elongator Met-tRNAs (Marck and Grosjean 2002; Kolitz and Lorsch 2010). Among them, whatever the domain of life, $tRNA_i^{Met}$ harbors a weak base pair or unpaired bases at position 1–72 whereas most elongator tRNAs possess a strong G–C base pair at this position. In bacteria, a conserved mismatch at position 1:72 (most frequently C_1:A_{72}) is involved in the recognition of Met-$tRNA_f^{Met}$ by methionyl-$tRNA_f^{Met}$ transformylase, the enzyme responsible for the formylation of the esterified methionine. However, biochemical studies have shown that a weak base pair was tolerated by the enzyme (Guillon et al. 1992). Indeed, the specific interaction of methionyl-$tRNA_f^{Met}$ transformylase with a methionylated initiator tRNA is based on the ability of the enzyme to open the 1–72 pair (Schmitt et al. 1998). Moreover, the absence of strong base-pairing at position 1–72 of the initiator tRNA was shown to be important for the rejection of the initiator tRNA by the elongation factor EF-Tu (Lee et al. 1991; Guillon et al. 1992; Rudinger et al. 1996) as well as for the protection of formyl-Met-$tRNA_f^{Met}$ against hydrolysis by peptidyl-tRNA hydrolase (Schulman and Pelka 1975; Dutka et al. 1993).

In eukaryotes and in archaea, Met-$tRNA_i^{Met}$ binds to the small ribosomal subunit as a complex with the heterotrimeric factor e/aIF2 in its GTP-bound form. When pairing between AUG codon and CAU anticodon is correct, e/aIF2 is released from the ribosome in a GDP-bound state. Therefore, the selection of the start codon is achieved through the control of the nucleotide state of e/aIF2. Eukaryotic and archaeal initiator tRNAs almost systematically carry an A_1–U_{72} base pair (one exception in *Schizosaccharomyces pombe* $tRNA_i^{Met}$

[1]**These authors contributed equally to this work.**

Corresponding author: emmanuelle.schmitt@polytechnique.edu

Article is online at http://www.rnajournal.org/cgi/doi/10.1261/rna.057877.116.

carrying a Ψ_1–A_{72} base pair ([Keith et al. 1993; Marck and Grosjean 2002]). This base pair has been shown crucial for the initiation process in various studies (von Pawel-Rammingen et al. 1992; Farruggio et al. 1996; Kapp and Lorsch 2004; Yatime et al. 2004; Kapp et al. 2006). By analogy with the interaction of methionyl-tRNA$_f^{Met}$ transformylase with Met-tRNA$_f^{Met}$ in bacteria, it was proposed that the opening of the 1–72 pair was important to ensure correct binding of the tRNA$_i^{Met}$ to e/aIF2 (Yatime et al. 2004). However, by studying Met-tRNA$_i^{Met}$ affinity for *S. cerevisiae* eIF2–GTP or eIF2–GDP, it was proposed that the identity and/or geometry of the 1–72 base pair was important for positioning the methionine moiety of the initiator tRNA in its recognition pocket and that an easily disrupted base pair may not be sufficient to ensure full binding specificity (Kapp and Lorsch 2004). Finally, beyond its function in e/aIF2 recognition, the A_1–U_{72} base pair was also shown to influence the binding of the ternary complex to the 40S subunit and later steps in translation initiation (Kapp et al. 2006). The available structure of the archaeal ternary complex (TC), aIF2:GTP:tRNA, revealed the positioning of the initiator tRNA with respect to aIF2. However, the resolution (5 Å) was too low to reveal the details of atomic interactions involving the A_1–U_{72} pair (Schmitt et al. 2012).

Structural studies of e/aIF2:tRNA, and more generally of eukaryotic and archaeal translation initiation complexes, would benefit from the availability of large amounts of pure initiator tRNA carrying an A_1–U_{72} base pair. Toward this aim, we are using an *E. coli* tRNA$_f^{Met}$$A_1$–$U_{72}$ variant as a good mimic of archaeal initiator tRNAs. To obtain pure fractions of such a tRNA, we designed an *E. coli* strain in which the four genes encoding initiator tRNA, *metZWV* and *metY* are inactivated and complemented by a plasmid-borne gene coding for the *E. coli* tRNA$_f^{Met}$$A_1$–$U_{72}$ variant as the sole source of initiator tRNA. We purified from this new strain large amounts of tRNA$_f^{Met}$$A_1$–$U_{72}$ devoid of wild-type tRNA$_f^{Met}$. This mutant tRNA, aminoacylated with methionine, was crystallized and the structure was solved and refined to 2.8 Å resolution. Interestingly, we find that A_1 adopts an unexpected *syn* conformation and forms a single H-bond interaction with U_{72}. This interaction requires protonation of the N1 atom of A_1. Moreover, the 5′ phosphoryl group folds back into the major groove of the acceptor stem and interacts with the N7 atom of G_2. A possible role of the peculiar geometry of the A_1–U_{72} base pair in the selection of the initiator tRNA by eukaryotic and archaeal translation initiation systems is discussed.

RESULTS

E. coli tRNA$_f^{Met}$$A_1$–$U_{72}$ resembles archaeal tRNA$_i^{Met}$

Sequences of archaeal tRNA$_i^{Met}$ were extracted from the tRNAscan-SE database (Lowe and Eddy 1997). A sequence logo (Schneider and Stephens 1990; Crooks et al. 2004) calculated from a multiple alignment of the 170 extracted DNA sequences shows a high level of conservation among archaeal initiator tRNA sequences (Fig. 1). For instance, *S. solfataricus* tRNA$_i^{Met}$ deviates from the consensus by only 13 positions. Interestingly, the sequence of a mutated *E. coli* Met-tRNA$_f^{Met}$ carrying A_1–U_{72} instead of C_1:A_{72} appears to be close to the archaeal consensus, with 13 deviations only (83% identity). In particular, the sequences of the acceptor stems are identical. Therefore, the *E. coli* tRNA$_f^{Met}$$A_1$–$U_{72}$ variant appears to be a good mimic of an archaeal initiator tRNA$_i^{Met}$.

Construction of a strain for tRNA$_f^{Met}$$A_1$–$U_{72}$ expression

A strain using pBSTNAV-tRNA$_f^{Met}$$A_1$–$U_{72}$ as its sole source of initiator tRNA was constructed in three steps: knockdown

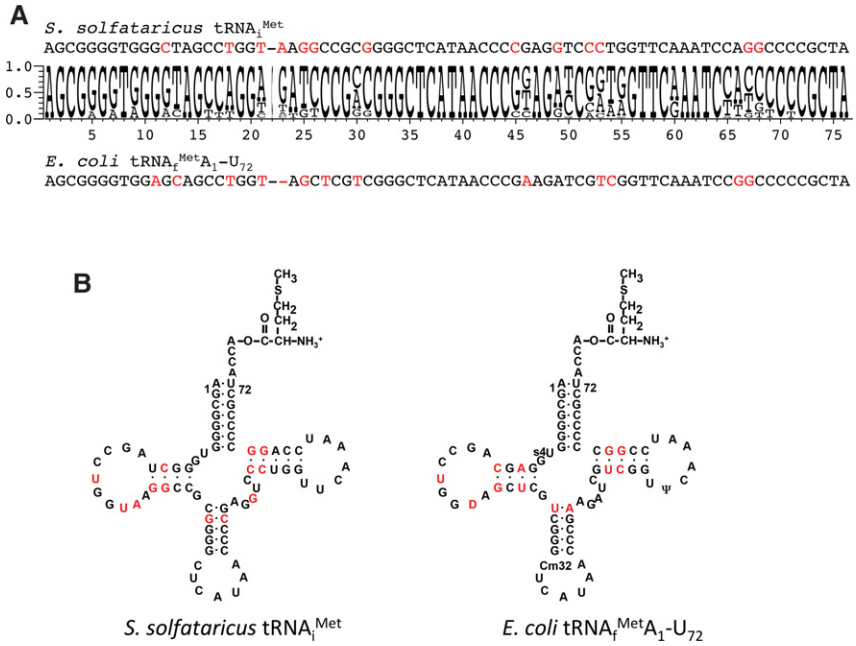

FIGURE 1. Comparison of archaeal initiator tRNAs with the *E. coli* tRNA$_f^{Met}$ A_1–U_{72} variant. (*A*) Sequences of archaeal tRNA$_i^{Met}$ were extracted from the tRNAscan-SE database (Lowe and Eddy 1997). A sequence logo calculated from a multiple alignment of the 170 DNA sequences obtained is shown. The DNA sequence of the *S. solfataricus* tRNA$_i^{Met}$ is shown *above* the logo and that of *E. coli* Met-tRNA$_f^{Met}$$A_1$–$U_{72}$ variant is shown *below*. Nucleotidic bases differing from the consensus sequence are in red. (*B*) Cloverleaf representations of initiator Met-tRNAs^{Met}. (*Left*) *S. solfataricus* Met-tRNA$_i^{Met}$, (*right*) *E. coli* Met-tRNA$_f^{Met}$$A_1$–$U_{72}$ variant. Note that wild-type tRNA$_f^{Met}$ carries C_1:A_{72}. Nucleotides differing from the archaeal initiator tRNA consensus are in red. Post-transcriptional modifications of *S. solfataricus* Met-tRNA$_i^{Met}$ are not known.

of *metZWV*, transformation by pBSTNAV-$tRNA_f^{Met}A_1$–U_{72} and knockdown of *metY*. First, the *metZWV* genes were deleted in *E. coli* MG1655 strain (Guyer et al. 1981). For this purpose, we have used the modified λRed/FLP procedure (Datsenko and Wanner 2000; Chen et al. 2015). The whole knockout procedure involved λRed recombinase-mediated replacement of the *metZWV* region by a *kan* marker flanked by two FRT sequences, one of which is mutated (Senecoff et al. 1988). The *kan* marker was then eliminated through FLP recombinase mediated reaction. The advantage of this procedure is that the mutant FRT sequence remaining on the chromosome at the knocked-out locus cannot react with any other FRT during subsequent modifications (Chen et al. 2015). Because of this and of the removal of the *kan* marker, the whole procedure can be repeated for knocking-out other genes. Recombination events were verified using PCR (Fig. 2A). The resulting strain PalΔmetZWV could grow because intiator tRNA was produced from the intact *metY* locus, as previously observed (Kenri et al. 1991; Kapoor et al. 2011; Samhita et al. 2012). However, it displayed a slow growth phenotype, yielding small colonies, in agreement with previous studies of a Δ*metZWV::kan* strain (Fig. 2B; Samhita et al. 2014). In contrast, when we deleted *metY* using the same procedure, normal growth of the obtained PalΔmetY strain was observed.

In order to knock out the *metY* gene in PalΔmetZWV, cells were transformed with the λRed-producing plasmid pKD46 (Datsenko and Wanner 2000) and then with pBSTNAV-$tRNA_f^{Met}A_1$–U_{72}. Introduction of the latter plasmid restored standard colony size, suggesting that the overproduced $tRNA_f^{Met}A_1$–U_{72} was functional in translation initiation (Fig. 2B). Interestingly, standard colony sizes were also restored with pBSTNAV-*S. solfataricus*-$tRNA_i^{Met}A_1$–U_{72} (Fig. 2B). Accordingly, the *metY* locus was successfully knocked-out through its λRed-mediated replacement by the *kan* gene. The obtained *E. coli* strain, PalΔmetZWVΔmetY::kan: pBSTNAV-$tRNA_f^{Met}A_1$–U_{72}, has $tRNA_f^{Met}A_1$–U_{72} as its sole source of initiator tRNA.

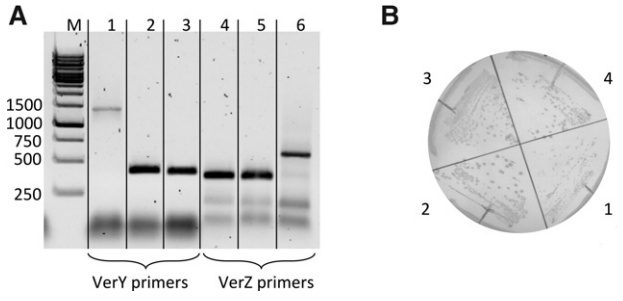

FIGURE 2. Inactivation of *metZWV* leads to a slow growth phenotype. (*A*) Verification by PCR of gene inactivation. The *metY* and *metZ* loci of each strain were probed by PCR analysis using whole cells as template DNA sources. Primer couples for probing the *metY* locus (VerY, lanes *1*,*2*,*3*) or the *metZ* locus (VerZ, lanes *4*,*5*,*6*). Shown are the analyses of PalΔmetZWVΔmetY:kanR-pBSTNAV2-$tRNA_f^{Met}A_1$–U_{72} (lanes *1*,*4*), PalΔmetZWV (lanes *2*,*5*), and PalΔmetY (lanes *3*,*6*). Expected sizes (after knockdown) are 1411 base pairs (bp) (lane *1*), 406 bp (lane *2*), 398 bp (lane *3*), 364 bp (lanes *4*,*5*), and 591 bp (lane *6*). Lane *M* was loaded with a molecular weight marker (MWD-1, Nippongenetics), relevant band sizes of which are indicated on the *left*. (*B*) Strain PalΔmetZWV transformed with PBSTNAV2 displays a slow growth phenotype (small colonies, 1). The phenotype can be reversed upon expression of either $tRNA_f^{Met}$ (2), $tRNA_f^{Met}A_1$–U_{72} (3), or *S. solfataricus* $tRNA_i^{Met}$ (4).

Overall structure of $tRNA_f^{Met}A_1$–U_{72} and crystal packing analysis

The strain described above was then used to overexpress and purify Met-$tRNA_f^{Met}A_1$–U_{72} for use in crystallization trials. Crystals belonging to space group $C222_1$ were obtained using 20% PEG 6000 and 2 M NaCl as precipitants. The structure was solved by molecular replacement and refined to 2.8 Å resolution. All bases are visible except C_{75} and the methionylated A_{76}.

An analysis using DSSR (Lu et al. 2015) identifies all the secondary structure elements characteristic of the classical cloverleaf secondary structure as well as usual tertiary interactions that stabilize the L-shaped tertiary fold of the molecule. A global superimposition of the present structure to that of wild-type *E. coli* $tRNA_f^{Met}$ (PDB entry 3CW5) (Barraud et al. 2008) shows modification in the angle made by the two branches of the tRNA, i.e., the anticodon helix (from P_{56} to P_{35}) and the acceptor helix (from P_{56} to P_{73}) as defined (Giege 2008). The angle varies from 71° for *E. coli* $tRNA_f^{Met}$ to 81° for $tRNA_f^{Met}A_1$–U_{72}. This difference reflects tRNA plasticity. For instance, the angle of the two tRNA branches varies from 110° to 65° in free and AspRS-bound $tRNA^{Asp}$ (Ruff et al. 1991). Crystals containing $tRNA_f^{Met}A_1$–U_{72} have been obtained in space group $C222_1$, whereas previous crystals of wild-type *E. coli* $tRNA_f^{Met}$ had been obtained in space group $P6_422$. In the present crystals, three regions of the tRNA are involved in packing interactions (Fig. 3). One contact point involves the anticodon loops of two tRNA molecules. Within this region, anticodon–anticodon base-pairing between the $C_{34}A_{35}U_{36}A_{38}$ nucleotides of one molecule and the corresponding nucleotides in a symmetry-related molecule is observed (Fig. 3A). Two Watson–Crick A–U pairs and two noncanonical C–A hydrogen bonds are holding this interaction. Notably, the same packing of anticodon loops was observed in $P6_422$ crystals of wild-type *E. coli* $tRNA_f^{Met}$ (Barraud et al. 2008).

A second contact point, specific to $C222_1$ crystals, involves the universal G_{19}–C_{56} base pair located at the elbow of the tRNA. The G_{19}–C_{56} base pair presents a flat hydrophobic surface stacked on the corresponding base pair of a neighboring tRNA molecule (Fig. 3B). This surface at the elbow is exploited for tRNA recognition by many partners including the ribosome (Korostelev et al. 2006; Zhang and Ferre-D'Amare 2013, 2016).

Finally, a third contact point, also specific to $C222_1$ crystals, exists between the top of the acceptor stem of one molecule and the minor groove of the T-stem of a neighbor. In

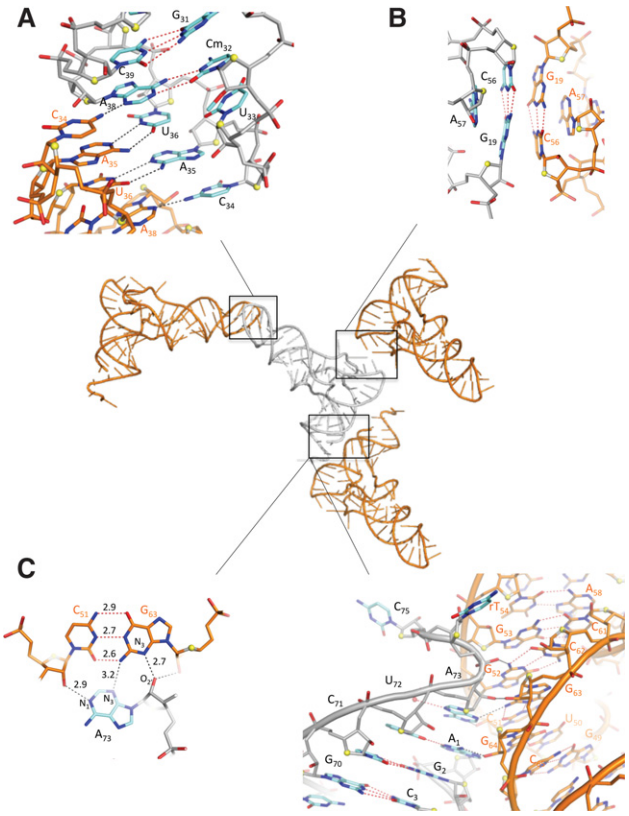

FIGURE 3. Crystal packing interactions. The *central* view shows arrangement of the tRNA molecules within the $C222_1$ crystals with the three contact points boxed and detailed in the close-up views. The reference molecule of the asymmetric unit is in gray and the neighboring molecules are in orange. In the close-up views, one molecule is shown with bases in cyan and the neighboring molecule is in orange. Intramolecular interactions are drawn with red dashed lines and intermolecular interactions are drawn with black dashed lines. Note that the close-up views are not drawn in the same orientations as the central view. (*A*) Crystal packing at the anticodon loop. (*B*) Crystal packing at the elbow. (*C*) Crystal packing at the *top* of the acceptor stem. The *left* view shows A_{73} of a tRNA molecule making an A-minor interaction with the C_{51}–G_{63} pair of a neighboring molecule. Distances are given in Å. The *right* view shows interaction of the acceptor stem of a tRNA molecule with the T-stem of a crystallographic neighbor. rT stands for ribothymidine.

particular, A_{73} makes an A-minor type I interaction (Nissen et al. 2001) with the G_{51}–C_{63} receptor base pair (Fig. 3C) as observed in a variant of group I self-splicing intron (Battle and Doudna 2002). A second interaction involves the NH_2 group of A_1 and the 2′OH group of a neighboring G_{64}. Also, one phosphate oxygen of C_{74} is bound to the NH_2 group of G_{52}.

Conformation of the anticodon stem–loop

The structure of the anticodon stem and loop is identical to that described for *E. coli* $tRNA_f^{Met}$ (Barraud et al. 2008). A_{37} protrudes outside of the anticodon loop and A_{38} is directly stacked onto U_{36}. An unusual Cm_{32}–A_{38} base pair is formed thereby extending the anticodon stem and restricting the anticodon loop to 5 nt. The Cm_{32}–A_{38} base pair is stabilized by a polar interaction between the N1 atom of A_{38} and the O2 atom of Cm_{32} and by stacking onto G_{31}–C_{39}. Finally, A_{37} is positioned within the major groove of the anticodon stem and forms a base triple with G_{29}–C_{41} (Fig. 4), as previously observed (Barraud et al. 2008). Superimposition of $tRNA_f^{Met}$ and $tRNA_f^{Met}A_1$–U_{72} structures shows that bending of the anticodon loops slightly differ. However, despite this movement, the network of interactions in the anticodon loop is conserved in the two tRNA structures.

An unusual A_1–U_{72} pair

Characteristic of eukaryotic and archaeal initiator tRNAs, the A_1–U_{72} pair at the top of the acceptor stem, shows a peculiar conformation (Fig. 5). Watson–Crick (WC) interactions between A_1 and U_{72} are unexpectedly not observed. When compared to a standard G_1–C_{72} WC base pair, as in $tRNA^{Phe}$ (PDB entry 1EHZ [Shi and Moore 2000]), a rotation of the A_1 base around bond P–O3′ is observed. Moreover, instead of adopting the usual *anti* conformation, the adenine ring rotates around the glycosidic bond and adopts a *syn* conformation ($\chi = -14.9°$) (Fig. 5A,B). The 5′ phosphoryl group folds back into the major groove of the acceptor stem and interacts with the N7 atom of G2 (Fig. 5A,C). On the other hand, base U_{72} remains stacked onto C_{71} as in a canonical $tRNA^{Phe}$ acceptor stem. As a consequence, the opening parameter (Lu et al. 2015) of the A_1–U_{72} base pair becomes unusually high (153.42°). The NH_2 group of A_1 points toward the minor groove of the acceptor helix. An interaction between the N1 of A_1 and the O2 of U_{72} ($d = 3.0$ Å) is observed which requires protonation of the N1 atom of A_1. In addition, A_{73} is stacked onto A_1 instead of being stacked on the first base pair of the acceptor stem as in $tRNA^{Phe}$ (Fig.

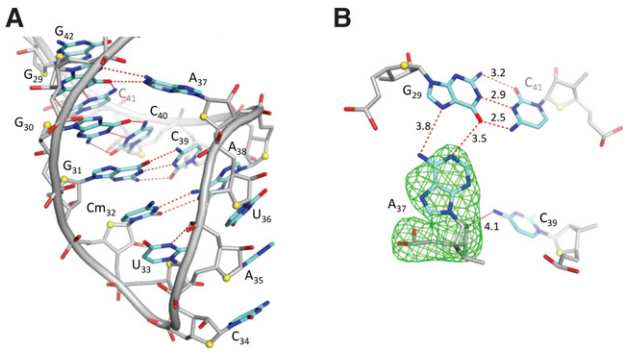

FIGURE 4. Conformation of the anticodon loop of the *E. coli* $tRNA_f^{Met}A_1$–U_{72} variant. (*A*) Global view of the anticodon loop of the *E. coli* $tRNA_f^{Met}A_1$–U_{72}. The figure shows A_{37} *outside* of the anticodon loop forming an A-minor interaction with the G_{29}–C_{41} base pair. A_{38} is stacked between U_{36} and C_{39} and forms an unusual base pair with Cm_{32}. (*B*) A_{37} (G_{29}–C_{41}) base triple. A simulated annealing mF_o–DF_c omit map contoured at 3.5 σ is shown for A_{37}. Distances are given in Å. They are consistent with hydrogen bonding within standard error on coordinates (Table 1).

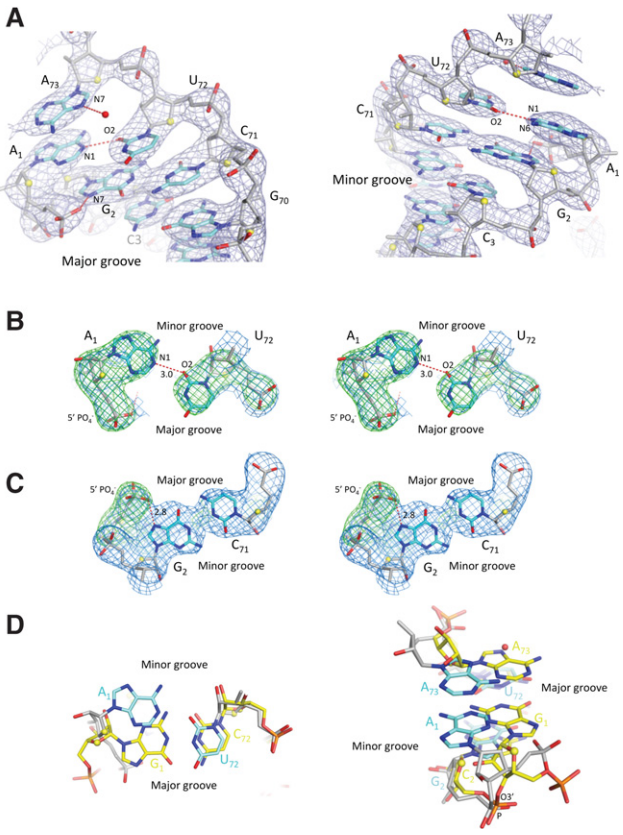

FIGURE 5. Conformation of the top of the acceptor stem of the *E. coli* $tRNA_f^{Met}A_1$–U_{72} variant. (*A*) Views in two orientations of the 2.8 Å resolution $2mF_o$–DF_c map of *E. coli* $tRNA_f^{Met}A_1$–U_{72} contoured at 2.5 SDs in the region of the A_1–U_{72} base pair. (*B*) Stereo view of the A_1–U_{72} base pair. Simulated annealing mF_o–DF_c (green) and $2mF_o$–DF_c (blue) omit maps contoured at 5 and 2.5 σ, respectively, are shown. (*C*) Stereo view showing interaction of the 5′PO4 group with N7 of G_2. Represented maps are the same as in panel *B*. The view shows that the 5′PO4 lies in the G_2–C_{71} plane. (*D*) The views in two different orientations compare the geometry of a standard G_1–C_{72} base pair as observed in $tRNA^{Phe}$ (yellow sticks, PDB entry 1EHZ [Shi and Moore 2000]) with that of the A_1–U_{72} base pair of *E. coli* $tRNA_f^{Met}A_1$–U_{72} (cyan sticks). Comparison results from the superimposition of the acceptor stems of the two tRNAs. The figures were drawn with Pymol (Schrodinger 2010).

5D). Finally, a water molecule bound to N7 of A_{73} located just above U_{72} could make an O–π or an H–π interaction with the uridine ring (Sarkhel et al. 2003). It is interesting to note that such water–nucleobase interactions would make up for the absence of base stacking on U_{72} (Fig. 5D).

Molecular dynamics simulation of a protonated A_1

In order to further study a possible relevance of the protonated state of A_1, molecular simulation techniques were used. Protonated N1 of adenine can be observed either in a neutral tautomer or in a positively charged form of the base. In a first step, we have evaluated a possible relevance of tautomeric forms of adenine using quantum chemistry methods (Warshel and Naray-Szabo 1997). The calculated relative energies of the adenine tautomers in solvent were 12.0 and 10.0 kcal/mol for the N6 proton being *cis* and *trans* relative to N1, respectively. These energies are high and do not depend on the medium pH. Therefore, neutral tautomers are not likely to be relevant. In a second step, we analyzed the stability of the positively charged form of adenine. The experimentally determined pK_a of N1 of adenine is 4.2 (Kampf et al. 2002). Therefore, the relative energy of the positively charged N1 protonated form of adenine is only 3.1 kcal/mol higher than the energy of the neutral form at a physiological pH of 6.5 suggesting that this form may exist in RNA complexes stabilized by favorable electrostatic interactions with negative phosphates. Therefore, in a second step, we used molecular dynamics simulations (Sham et al. 1997; Aleksandrov et al. 2007) to compute protonation free energies of adenine A_1 of $tRNA_f^{Met}A_1$–U_{72} in solution and in the crystal. Molecular dynamics was used to average values over the multiple conformations observed during the simulations and to model protonation states not observed in the crystal. The

TABLE 1. Data collection and refinement statistics for $tRNA_f^{Met}A_1$–U_{72} structure determination

Data collection[a]	$tRNA_f^{Met}A_1$–U_{72}
Space group	$C222_1$
Cell dimensions	
a, *b*, *c* (Å)	35.15 142.62 202.12
αβγ (°)	90 90 90
Resolution (Å)	41.2–2.8
R_{sym}[b,c] (%)	8.4 (246.4)
$I/\sigma I$	17.03 (0.95)
CC(1/2)[d] (%)	99.9 (74.4)
Completeness (%)	99.2 (95.5)
Redundancy	9.84 (9.74)
Refinement	
Resolution (Å)	35.2–2.8
No. of reflections	13,004
R_{work} (R_{free})[e]	0.196 (0.225)
No. of atoms/B-factors (Å^2)	
tRNA	1623/116.7
Water	5/92.8
Na^+	1/70.5
R.m.s. deviations	
Bond lengths (Å)	0.005
Bond angles (°)	1.14
Error estimates	
Coordinate error (Å)	0.38
Phase error (°)	28.6

[a]A single crystal was used for data collection.

[b]$R_{sym}(I) = \frac{\sum_{hkl}\sum_i |\langle I_{hkl}\rangle - I_{hkl,i}|}{\sum_{hkl}\sum_i |I_{hkl}|}$, where *i* is the number of reflections *hkl*.

[c]Values in parentheses are for highest-resolution shell.

[d]CC(1/2) is the correlation coefficient between two random half data sets (Karplus and Diederichs 2012).

[e]$R_{work} = \frac{\sum ||F_{obs}| - |F_{calc}||}{\sum |F_{obs}|}$.

R_{free} is calculated with 5% of the reflections.

structure of $tRNA_f^{Met}A_1$–U_{72} with the A_1–U_{72} pair observed in the crystal is stable during molecular dynamics simulation with A_1 in the N1 protonated form (Fig. 6A). This suggests that this conformation can exist in solution. In MD simulations with A_1 in the neutral form the A_1–U_{72} base pair adopts a reverse Watson–Crick conformation (Fig. 6B). We calculated protonation free energies using these MD simulations. For $tRNA_f^{Met}A_1$–U_{72} in solution, the protonation free energy for A_1 (2.2 kcal/mol) is lowered by 0.9 kcal/mol as compared to what is computed for free adenine. This corresponds to a pK_a value of 4.9 for the N1 of A_1 (see relationships between $\Delta\Delta G$ and pK_a in Materials and Methods). If the crystal environment is taken into account, the protonation of A_1 of $tRNA_f^{Met}A_1$–U_{72} is favored by an additional 0.9 kcal/mol, leading to a protonation free energy of 1.3 kcal/mol that corresponds to a pK_a of 5.6 for the N1 atom of A_1. Notably, further increase of the pK_a value may occur through interaction of an anion in the vicinity of A_1 that would not have been detected at the resolution reached in the crystal structure.

DISCUSSION

The present work describes the construction of an *E. coli* strain able to grow in a genetic context where a variant of the initiator tRNA is used as the sole source of initiator tRNA. Using such a strain we observed that *E. coli* growth is supported by overexpression of an initiator tRNA carrying an A_1–U_{72} base pair instead of the natural C_1:A_{72}. This result is consistent with previous work showing that the absence of strong base-pairing at position 1–72 is sufficient to ensure efficient formylation of Met-$tRNA_f^{Met}$, an important step for initiation of translation (Guillon et al. 1993; Mangroo and Rajbhandary 1995). Because productive interaction with the formylase requires opening of the 1–72 bp, this shows the propensity of the A_1–U_{72} base pair to reach an open conformation. Accordingly, we observed that *E. coli* growth is supported by overexpression of the archaeal initiator $tRNA_i^{Met}$ from *S. solfataricus*, a tRNA having a sequence very close to that of an *E. coli* $tRNA_f^{Met}A_1$–U_{72} variant (Fig. 1B). Hence, the λRed/FLP procedure applied on PalΔmetZWV in the presence of an overproducing initiator tRNA plasmid gives a useful tool to test for initiator tRNA complementation and to allow for overexpression and efficient purification of effective initiator tRNA variants in an *E. coli* context. This method represents a useful alternative to the P1 transduction strategy (Samhita et al. 2012) in particular in cases where it is desirable to limit the number of antibiotic resistance genes.

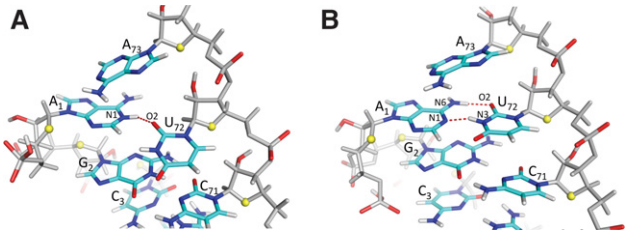

FIGURE 6. Final structures of the A_1–U_{72} base pair after 5 nsec of MD simulations of $tRNA_f^{Met}A_1$–U_{72} in the crystal environment with A_1 in the N1 protonated form (*A*) and with A_1 in the neutral form (*B*).

Using pure fractions of the *E. coli* $tRNA_f^{Met}A_1$–U_{72} variant, we obtained crystals and solved the 3D structure of the tRNA. The overall structure presents all the tertiary interactions responsible for the L-shaped folding of the tRNA as previously described (Barraud et al. 2008). Two regions exhibit specific structural features: the anticodon loop and the top of the acceptor stem. Within the anticodon loop, A_{37} is extruded and A_{38} makes a peculiar base pair with Cm_{32}. Notably, the unusual conformation of the anticodon region was already observed in wild-type $tRNA_f^{Met}$ crystals obtained in a different space group (Barraud et al. 2008). In this view, it is notable that yeast initiator tRNA also shows an extruded base 37 (Basavappa and Sigler 1991). However, in this case, the presence of an N6-threonylcarbamoyladenosine modification in A_{37} might explain the absence of a base triple interaction between t_6A_{37} and the G_{29}–C_{41} base pair. Together, these structures reflect the propensity of the anticodon loop of initiator tRNAs to adopt a "37-unstacked" conformation. This observation reinforces the idea that the switch between a "37-unstacked" conformation observed in free-initiator tRNAs (present work; Basavappa and Sigler 1991; Barraud et al. 2008) as compared to the "37-stacked" conformation observed in $tRNA_f^{Met}$ bound to the P site (Selmer et al. 2006) might be important for initiator tRNA selection during the translation initiation process.

At the top of the acceptor stem, $tRNA_f^{Met}A_1$–U_{72} shows an unusual conformation of the A_1–U_{72} pair. Bases A_1 and U_{72} are systematically encountered in archaeal initiator tRNAs and only one exception is known in eukaryotic initiator tRNAs (Marck and Grosjean 2002). Recent biochemical results have suggested that the identity of the A_1–U_{72} base pair was important to ensure the correct selection of the initiator tRNA during translation initiation and that a weak base pair at position 1:72 was not sufficient (for review, see Kolitz and Lorsch 2010). In eukaryotes and in archaea, the initiator tRNA is delivered to the ribosome as a ternary complex, e/aIF2:GTP:tRNA. In the TC, it was suggested that the geometry of the base pair at 1–72 was important for the correct positioning of the methionine moiety in its binding pocket (Kapp and Lorsch 2004). Furthermore, it was also proposed that the A_1–U_{72} base pair plays a role in the binding of the TC within the translation initiation complex and directly affects translation efficiency (Kapp et al. 2006).

Notably, interaction of the N1 atom of A_1 with the O2 atom of U_{72} ($d = 3.0$ Å) assumes that N1 of A_1 is protonated. In the present study, crystals have been obtained at pH 6.3, a pH where the N1 of adenosine is normally not protonated (Saenger 1984). In order to evaluate the relevance of the peculiar conformation of the A_1–U_{72} pair, we performed a

computational study of the protonation state of A_1 using molecular simulation techniques. As expected (Fonseca Guerra et al. 2006), the results of the calculations make it unlikely that the occurrence of adenine tautomers play a significant role in the observed conformation. However, formation of a positively charged A_1 through protonation of the N1 atom has a much lower energetic cost. Several conclusions may be drawn from the calculations. First, the energetic penalty for protonation of N1 of A_1 is not very high (2.2 kcal/mol in solution or 1.3 kcal/mol in the crystal). Second, crystal packing does not seem to have a predominant influence on the decrease of the free energy necessary for protonation because it contributes 0.9 kcal/mol only. Finally, the structure of $tRNA_f^{Met}A_1$–U_{72} observed here is stable during molecular dynamics simulations with protonated A_1. Therefore, the unusual conformation observed here must exist at least transiently in solution. Accordingly, the crystals are able to nucleate and grow. Overall, these calculations strongly suggest that interaction of the A_1–U_{72} base pair with a proteic partner could easily stabilize a structure of the $tRNA_f^{Met}$ with the peculiar A_1–U_{72} arrangement observed in the crystal including protonation of N1 of A_1. pK_a value shifting toward neutrality explained by electrostatic stabilization has been observed, for instance, in specific bases of ribozymes (Ravindranathan et al. 2000; Wilcox et al. 2011; Liberman et al. 2012) or in $tRNA_3^{Lys}$ anticodon stem–loop (Durant and Davis 1999).

One obvious candidate for the stabilization of the unusual A_1–U_{72} base pair is e/aIF2-GTP within the TC. In this view, the peculiar A_1–U_{72} conformation might explain its role in the positioning of the methionine moiety of the initiator tRNA in its recognition pocket within the γ subunit of eIF2-GTP (Kapp and Lorsch 2004). Notably, the crystal structure of nonaminoacylated *S. cerevisiae* initiator tRNA, obtained in the $P6_422$ space group, shows a standard WC A_1–U_{72} base pair (Basavappa and Sigler 1991). In the present study, the use of a methionylated tRNA may have influenced the conformation of the A_1–U_{72} base pair. Notably, attempts to obtain crystals of nonaminoacylated $tRNA_f^{Met}A_1$–U_{72} in the same conditions were unsuccessful. However, a possible influence of the methionyl moiety remains unlikely because the C_{75} and met-A_{76} bases are disordered in the crystal. Nevertheless, the fact that the A_1–U_{72} base pair can be easily opened suggests that the closing base pair of the initiator tRNA may switch between different conformations depending on its partners at the various stages of its functional cycle. Unfortunately, the available 3D structure of archaeal TC aIF2:GDPNP:Met-$tRNA_f^{Met}$ was obtained at low resolution (5Å) thus preventing observation of the fine geometrical requirements for optimal tRNA binding (Schmitt et al. 2012). Therefore, further structural studies of the TC are required to reveal the conformation of the A_1–U_{72} base pair of the initiator tRNA bound to e/aIF2. Finally, recent Cryo-EM studies of archaeal translation initiation complexes (Coureux et al. 2016) show transient deformation of the TC structure at some stages of the translation initiation process. Resolutions of the cryo-EM structures were not sufficient to observe the status of the A_1–U_{72} base pair. It is, however, conceivable that adjustments of the A_1–U_{72} base pair geometry participate in the control of the dynamics of the initiation complex during start codon recognition. To conclude, the present work gives a new example of an RNA structure with rare ionic forms of bases that could be important for RNA function (Wilcox et al. 2011; Liberman et al. 2012; Rozov et al. 2016).

MATERIALS AND METHODS

Inactivation of genes in the *E. coli* chromosome

Gene deletions were performed using the λRed/FLP procedure (Datsenko and Wanner 2000) as modified (Chen et al. 2015). *E. coli* K12 MG1655 strain (F^- λ^- *ilvG*$^-$ *rfb*-50 *rph*-1) was transformed with the pKD46 plasmid, carrying a thermosensitive replicon and the λ *Red* operon under the control of an arabinose inducible promoter. Cells were plated on LB plates supplemented with ampicillin (50 μg/mL) and grown at 30°C. The *kan* gene flanked by FRT (Flp recombinase Recognition Target) sequences carried by pEAW507 was PCR-amplified using primers made of approximately 50 bases immediately adjacent to the region to be deleted fused to 19 bases bordering the FRT-kan-FRT cassette on the plasmid. Sequences of the oligonucleotides used for the deletions of *metZWV* and *metY* were as follows :

5′AAAAAAAGGTTGCATGAAAACGCGAGCGGAGTATAGTGC GCATCCACGGACGTAGAGGATCCCGGAAGT3′ (*metZWV*-forward)

5′TTTATGGGAGACCAGAAACAAAAAAACACCCGTTAGGGT GTTCAATAATTCCCTTTCGTCTTCAAGAAT3′ (*metZWV*-reverse)

5′GCAGTATTTGCATTTTTTACCCAAAACGAGTAGAATTTGCC ACGTTTCAGGCGTAGAGGATCCCGGAAGT3′ (*metY*-forward)

5′CGAAGGCCGAAGTCTTCACAGTATATTTGAAAAAGGACTC TAAGGGAAAGCCCTTTCGTCTTCAAGAAT3′ (*metY*-reverse)

The PCR product was digested by DpnI in order to degrade the plasmid template, and transformed by electroporation into MG1655-pKD46 cells grown at 30°C in LB medium containing 1 mM L-arabinose. After electroporation, 1 mL of LB medium containing 1 mM L-arabinose was added and cells were incubated 2 h at 30°C plus 4 h at 37°C, and finally plated at 37°C on LB plates containing kanamycin (25 μg/mL). Clones were then tested by PCR for correct recombination of the cassette at the desired locus and for loss of the pKD46 plasmid. PCR primers were as follows: 5′GGCGCAAC GAAGATAACAAACCGCCGC3′ (ver-*metZWV*-forward), 5′GTAT TTTGCGATGGGGCGACGTGGCGA3′ (ver-*metZWV*-reverse), 5′AGTATTCAACAAATGAAAGTGAACTGG3′ (ver-*metY*-forward), and 5′TAACAAAAAACCCCGATAAATCGGGGC3′ (ver-*metY*-reverse).

For elimination of the *kan* gene, cells were first transformed with pLH29 (Huang et al. 1997), a plasmid expressing the FLP recombinase. One colony was grown overnight at 37°C in 20 mL of LB containing 25 μg/mL chloramphenicol and 1 mM IPTG, and then left 2 d at room temperature. Clones were then screened for loss of resistance to kanamycin, and removal of the *kan* gene was then verified

by PCR using the primers described above (Fig. 2A). Finally, plasmid pLH29 was eliminated by performing four successive liquid cultures to saturation in LB at 37°C. Individual clones were finally tested for loss of pLH29 by assaying sensitivity to chloramphenicol. This procedure yielded PalΔmetZWV and PalΔmetY strains.

For inactivation of *metY* in PalΔmetZWV carrying pBSTNAV-tRNA$_f^{Met}$A$_1$–U$_{72}$ derivative, the same procedure was used except that pKD46 was selected with gentamicin instead of ampicillin. In this case, the *kan* gene at the *metY* locus was not removed after *metY* deletion. This procedure yielded PalΔmetZWVΔmetY::kan strains carrying a pBSTNAV-tRNA$_f^{Met}$A$_1$–U$_{72}$.

tRNA purification

The *E. coli* tRNA$_f^{Met}$A$_1$–U$_{72}$ variant was overexpressed in PalΔmetZWVΔmetY::kan carrying pBSTNAV-tRNA$_f^{Met}$A$_1$–U$_{72}$ and purified as previously described (Mechulam et al. 2007). Briefly, a whole tRNA extract was prepared according to the Zubay procedure (Zubay 1962). The overexpressed tRNA$_f^{Met}$ was then separated from other tRNAs by an anion exchange step on a Q-Hiload column (16 × 100 mm) equilibrated in 20 mM Tris–HCl, pH 7.6, 200 mM NaCl, 8 mM $MgCl_2$, 0.1 mM EDTA. tRNAs were eluted using a 350 mM to 550 mM NaCl gradient in the same buffer. About 10 mg of tRNA$_f^{Met}$A$_1$–U$_{72}$ was obtained from 1 L of *E. coli* culture. Methionine acceptance of the tRNA$_f^{Met}$A$_1$–U$_{72}$ preparation ranged between 1450 and 1600 pmol/A$_{260}$ unit. Before crystallization, the tRNA was methionylated and purified as described in Mechulam et al. (2007). The aminoacylated tRNA was resuspended in water (final concentration 400 μM) and diluted to 50 μM in a buffer containing 10 mM MOPS, pH 6.7, 5 mM $MgCl_2$, 200 mM NaCl, 10 mM 2-mercaptoethanol before crystallization trials.

Crystallization, data collection, structure solution, and refinement

Crystals belonging to space group C222$_1$ were obtained using the sitting drop method with a 1:1 mixture of a 50 μM solution of Met-tRNA$_f^{Met}$A$_1$–U$_{72}$ and 20% PEG 6000, 2 M NaCl as precipitants. Final pH of the 1:1 mixture of tRNA and precipitant was 6.3. Interestingly, the C222$_1$ space group was never observed for crystals of wild-type *E. coli* initiator tRNA$_f^{Met}$. According to the CC(1/2) values (Table 1) the high-resolution limit of the data set was 2.8 Å (Karplus and Diederichs 2012; Diederichs and Karplus 2013). The structure was solved by molecular replacement using PHASER and the coordinates of *E. coli* tRNA$_f^{Met}$ (PDB entry 3CW5 [Barraud et al. 2008]) from which the terminal CCA bases have been removed. Initial map showed different orientations of the anticodon region and of the 3′ extremity of the acceptor helix as compared to the molecular replacement-starting model. Cycles of manual reconstructions, performed with the program COOT (Emsley et al. 2010), and of refinements steps with PHENIX (Adams et al. 2010), led to a model refined to 2.8 Å resolution (R_{work} = 0.196, R_{free} = 0.225). Because of crystal packing interactions, the tRNA molecules are more tightly bound together along the acceptor helices. This is reflected by lower B-values along the acceptor helix comparing with those observed for atoms belonging to the anticodon helix. According to this anisotropy, the TLS procedure (Adams et al. 2010) was used in the last steps of refinement. All nucleotides are visible except A$_{76}$. Moreover, positioning of C$_{75}$ is only tentative. Refinement parameters in Table 1 were calculated with PHENIX.

Relative stability of adenine tautomers in solvent

The structures of adenine tautomers were energetically optimized at the density functional theory (DFT) level with the ORCA program version 3.0 (Neese 2012). The TPSS (Tao et al. 2003) functional and the Ahlrich's def2-TZVP AO basis set (Weigend and Ahlrichs 2005) were used. Single-point energy calculations at the higher level of theory, second-order Møller–Plesset perturbation (MP2), using the same basis set were performed on the minimized structures. The implicit solvent calculations were performed within the COSMO conductor-like screening model (Eckert and Klamt 2002) with a dielectric constant of ε = 80.0.

Molecular dynamics simulations

The simulations included tRNA nucleotides within a 24 Å sphere, centered on the A$_1$ nucleotide of tRNA. tRNA atoms between 20 and 24 Å from the sphere's center were harmonically restrained to their experimentally determined positions. A 75 Å cubic box of water was overlaid, and waters overlapping the RNA atoms were removed. Periodic boundary conditions were assumed, i.e., the entire 75 Å box was replicated periodically in all directions. All long-range electrostatic interactions were computed efficiently by the particle mesh Ewald method (Darden 2001) and the appropriate number of potassium counterions were included to render the system electrically neutral. MD simulations were performed at constant room temperature and pressure, after 200 ps of thermalization. The CHARMM27 force field was used for the tRNA (Foloppe and MacKerell 2000) and the TIP3 model for water (Jorgensen et al. 1983). For the protonated form of adenine, we used a force field specifically developed in this work. Calculations were done with the NAMD program (Phillips et al. 2005). Ten nanoseconds of molecular dynamics were performed at constant room temperature and pressure.

To model residue A$_1$ of tRNA in the crystalline environment, the symmetric units were constructed according to the crystallographic symmetry operators. Nucleotides within a 24 Å sphere around nucleotide A$_1$ were retained for simulations. The rest of the system preparation was identical to the setup used for the simulations of tRNA in solvent.

Poisson–Boltzmann linear response approximation (PBLRA)

For the protonation free energy of the A$_1$ adenine of tRNA in solution and in crystal, we used a simpler Poisson–Boltzmann linear response approximation, or PB/LRA (Aleksandrov et al. 2007). The protonation of the A$_1$ adenine was modeled by changing selected atomic charges. The corresponding free energy change was computed both in tRNA and for the adenine molecule alone in solution, using conformations taken from the last 2 ns of tRNA MD simulations. The free energy was approximated by the continuum electrostatic free energy, where the tRNA atoms are explicitly included but the solvent is replaced by a dielectric continuum. The

electrostatic potentials were computed for each MD conformation by numerically solving the Poisson–Boltzmann equation of continuum electrostatics (Aleksandrov et al. 2007), where the tRNA was treated as a single dielectric medium with a dielectric constant of 2; solvent was treated as another medium with a dielectric constant of 80, the experimental value for bulk water. The boundary between the two dielectric media was defined as the tRNA molecular surface, computed with a 1.6 Å radius probe sphere. For the potential calculation, the system was discretized using a cubic grid with a 68 Å edge and a spacing of 0.4 Å. The Poisson–Boltzmann equation was solved with Coulombic boundary conditions, using the CHARMM program (Brooks et al. 2009). We used an ionic strength corresponding to a 0.15 M concentration of monovalent ions.

The proton binding constant of A1 is related to $\Delta\Delta G$ by the relationship:

$$\mathrm{pKa_{tRNA}} = \mathrm{pKa_{adenine}} + \frac{1}{2.303\ kT}\ \Delta\Delta G_{A1(0)\rightarrow A1(+)},$$

where $\mathrm{pKa_{tRNA}}$ and $\mathrm{pKa_{adenine}}$ are the $\mathrm{pK_a}$ values of the titrating group in the tRNA and in the reference molecule, adenine, respectively.

DATA DEPOSITION

The Protein Data Bank accession number for the structure reported in this article is 5L4O.

ACKNOWLEDGMENTS

We thank the staff of the macromolecular crystallography beamlines PX1 and PX2 at the SOLEIL synchrotron (Saclay, France) for expert assistance during data collection. This work was supported by grants from the Centre National de la Recherche Scientifique and by Ecole polytechnique to Unité Mixte de Recherche no. 7654. A.M. was a recipient of a Gaspard Monge PhD fellowship from Ecole polytechnique.

Received June 10, 2016; accepted January 26, 2017.

REFERENCES

Adams PD, Afonine PV, Bunkóczi G, Chen VB, Davis IW, Echols N, Headd JJ, Hung LW, Kapral GJ, Grosse-Kunstleve RW, et al. 2010. *PHENIX*: a comprehensive Python-based system for macromolecular structure solution. *Acta Crystallogr D Biol Crystallogr* **66:** 213–221.

Aleksandrov A, Proft J, Hinrichs W, Simonson T. 2007. Protonation patterns in tetracycline:tet repressor recognition: simulations and experiments. *Chembiochem* **8:** 675–685.

Barraud P, Schmitt E, Mechulam Y, Dardel F, Tisné C. 2008. A unique conformation of the anticodon stem-loop is associated with the capacity of $tRNA_f^{Met}$ to initiate protein synthesis. *Nucleic Acids Res* **36:** 4894–4901.

Basavappa R, Sigler PB. 1991. The 3 Å crystal structure of yeast initiator tRNA: functional implications in initiator/elongator discrimination. *EMBO J* **10:** 3105–3111.

Battle DJ, Doudna JA. 2002. Specificity of RNA-RNA helix recognition. *Proc Natl Acad Sci* **99:** 11676–11681.

Brooks BR, Brooks CL III, Mackerell AD Jr, Nilsson L, Petrella RJ, Roux B, Won Y, Archontis G, Bartels C, Boresch S, et al. 2009. CHARMM: the biomolecular simulation program. *J Comp Chem* **30:** 1545–1614.

Chen SH, Byrne RT, Wood EA, Cox MM. 2015. *Escherichia coli radD (yejH)* gene: a novel function involved in radiation resistance and double-strand break repair. *Mol Microbiol* **95:** 754–768.

Coureux PD, Lazennec-Schurdevin C, Monestier A, Larquet E, Cladière L, Klaholz BP, Schmitt E, Mechulam Y. 2016. Cryo-EM study of start codon selection during archaeal translation initiation. *Nat Commun* **7:** 13366.

Crooks GE, Hon G, Chandonia JM, Brenner SE. 2004. WebLogo: a sequence logo generator. *Genome Res* **14:** 1188–1190.

Darden T. 2001. Treatment of long-range forces and potential. In *Computational biochemistry & biophysics* (ed. Becker O, et al.). Marcel Dekker, New York.

Datsenko KA, Wanner BL. 2000. One-step inactivation of chromosomal genes in *Escherichia coli* K-12 using PCR products. *Proc Natl Acad Sci* **97:** 6640–6645.

Diederichs K, Karplus PA. 2013. Better models by discarding data? *Acta Crystallogr D Biol Crystallogr* **69:** 1215–1222.

Durant PC, Davis DR. 1999. Stabilization of the anticodon stem-loop of $tRNA^{Lys,3}$ by an A^+-C base-pair and by pseudouridine. *J Mol Biol* **285:** 115–131.

Dutka S, Meinnel T, Lazennec C, Mechulam Y, Blanquet S. 1993. Role of the 1–72 base pair in tRNAs for the activity of *Escherichia coli* peptidyl-tRNA hydrolase. *Nucleic Acids Res* **21:** 4025–4030.

Eckert F, Klamt A. 2002. Fast solvent screening via quantum chemistry: COSMO-RS approach. *AlChE J* **48:** 369–385.

Emsley P, Lohkamp B, Scott WG, Cowtan K. 2010. Features and development of *Coot*. *Acta Crystallogr* **D66:** 486–501.

Farruggio D, Chaudhuri J, Maitra U, RajBhandary UL. 1996. The A1 • U72 base pair conserved in eukaryotic initiator tRNAs is important specifically for binding to the eukaryotic translation initiation factor eIF2. *Mol Cell Biol* **16:** 4248–4256.

Foloppe N, MacKerell A. 2000. All-atom empirical force field for nucleic acids: I. Parameter optimization based on small molecule and condensed phase macromolecular target data. *J Comput Chem* **21:** 86–104.

Fonseca Guerra C, Bickelhaupt FM, Saha S, Wang F. 2006. Adenine tautomers: relative stabilities, ionization energies, and mismatch with cytosine. *J Phys Chem A* **110:** 4012–4020.

Giege R. 2008. Toward a more complete view of tRNA biology. *Nat Struct Mol Biol* **15:** 1007–1014.

Guillon JM, Meinnel T, Mechulam Y, Lazennec C, Blanquet S, Fayat G. 1992. Nucleotides of tRNA governing the specificity of *Escherichia coli* methionyl-$tRNA_f^{Met}$ formyltransferase. *J Mol Biol* **224:** 359–367.

Guillon JM, Mechulam Y, Blanquet S, Fayat G. 1993. Importance of formylability and anticodon stem sequence to give $tRNA^{Met}$ an initiator identity in *Escherichia coli*. *J Bacteriol* **175:** 4507–4514.

Guyer MS, Reed RR, Steitz JA, Low KB. 1981. Identification of a sex-factor-affinity site in *E. coli* as γδ. *Cold Spring Harb Symp Quant Biol* **45** (Pt 1)**:** 135–140.

Huang HK, Yoon H, Hannig EM, Donahue TF. 1997. GTP hydrolysis controls stringent selection of the AUG start codon during translation initiation in *Saccharomyces cerevisiae*. *Genes Dev* **11:** 2396–2413.

Jorgensen W, Chandrasekhar J, Madura J, Impey R, Klein M. 1983. Comparison of simple potential functions for simulating liquid water. *J Chem Phys* **79:** 926–935.

Kampf G, Kapinos LE, Griesser R, Lippert B, Sigel H. 2002. Comparison of the acid-base properties of purine derivatives in aqueous solution. Determination of intrinsic proton affinities of various basic sites. *J Chem Soc Perkin Trans* **2:** 1320–1327.

Kapoor S, Das G, Varshney U. 2011. Crucial contribution of the multiple copies of the initiator tRNA genes in the fidelity of $tRNA_f^{Met}$ selection on the ribosomal P-site in *Escherichia coli*. *Nucleic Acids Res* **39:** 202–212.

Kapp LD, Lorsch JR. 2004. GTP-dependent recognition of the methionine moiety on initiator tRNA by translation factor eIF2. *J Mol Biol* **335:** 923–936.

Kapp LD, Kolitz SE, Lorsch JR. 2006. Yeast initiator tRNA identity elements cooperate to influence multiple steps of translation initiation. *RNA* **12:** 751–764.

Karplus PA, Diederichs K. 2012. Linking crystallographic model and data quality. *Science* **336:** 1030–1033.

Keith G, Heitzler J, el Adlouni C, Glasser AL, Fix C, Desgres J, Dirheimer G. 1993. The primary structure of cytoplasmic initiator $tRNA^{Met}$ from *Schizosaccharomyces pombe*. *Nucleic Acids Res* **21:** 2949.

Kenri T, Kohno K, Goshima N, Imamoto F, Kano Y. 1991. Construction and characterization of an *Escherichia coli* mutant with a deletion of the *metZ* gene encoding $tRNA_{f1}^{Met}$. *Gene* **103:** 31–36.

Kolitz SE, Lorsch JR. 2010. Eukaryotic initiator tRNA: finely tuned and ready for action. *FEBS Lett* **584:** 396–404.

Korostelev A, Trakhanov S, Laurberg M, Noller HF. 2006. Crystal structure of a 70S ribosome-tRNA complex reveals functional interactions and rearrangements. *Cell* **126:** 1065–1077.

Lee CP, Seong BL, RalBhandary UL. 1991. Structural and sequence elements important for recognition of *Escherichia coli* formylmethionine tRNA by methionyl-tRNA transformylase are clustered in the acceptor stem. *J Biol Chem* **266:** 18012–18017.

Liberman JA, Guo M, Jenkins JL, Krucinska J, Chen Y, Carey PR, Wedekind JE. 2012. A transition-state interaction shifts nucleobase ionization toward neutrality to facilitate small ribozyme catalysis. *J Am Chem Soc* **134:** 16933–16936.

Lowe TM, Eddy SR. 1997. tRNAscan-SE: a program for improved detection of transfer RNA genes in genomic sequence. *Nucleic Acids Res* **25:** 955–964.

Lu XJ, Bussemaker HJ, Olson WK. 2015. DSSR: an integrated software tool for dissecting the spatial structure of RNA. *Nucleic Acids Res* **43:** e142.

Mangroo D, Rajbhandary UL. 1995. Mutants of *Escherichia coli* initiator tRNA defective in initiation. *J Biol Chem* **270:** 12203–12209.

Marck C, Grosjean H. 2002. tRNomics: analysis of tRNA genes from 50 genomes of Eukarya, Archaea, and Bacteria reveals anticodon-sparing strategies and domain-specific features. *RNA* **8:** 1189–1232.

Mechulam Y, Guillon L, Yatime L, Blanquet S, Schmitt E. 2007. Protection-based assays to measure aminoacyl-tRNA binding to translation initiation factors. *Methods Enzymol* **430:** 265–281.

Neese F. 2012. The ORCA program system. *WIREs Comput Mol Sci* **2:** 73–78.

Nissen P, Ippolito JA, Ban N, Moore PB, Steitz TA. 2001. RNA tertiary interactions in the large ribosomal subunit: the A-minor motif. *Proc Natl Acad Sci* **98:** 4899–4903.

Phillips J, Braun R, Wang W, Gumbart J, Tajkhorshid E, Villa E, Chipot C, Skeel R, Kalé L, Schulten K. 2005. Scalable molecular dynamics with NAMD. *J Comput Chem* **26:** 1781–1802.

Ravindranathan S, Butcher SE, Feigon J. 2000. Adenine protonation in domain B of the hairpin ribozyme. *Biochemistry* **39:** 16026–16032.

Rozov A, Demeshkina N, Westhof E, Yusupov M, Yusupova G. 2016. New structural insights into translational miscoding. *Trends Biochem Sci* **41:** 798–814.

Rudinger J, Hillenbrandt R, Sprinzl M, Giege R. 1996. Antideterminants present in minihelix(Sec) hinder its recognition by prokaryotic elongation factor Tu. *EMBO J* **15:** 650–657.

Ruff M, Krishnaswamy S, Boeglin M, Poterszman A, Mitschler A, Podjarny A, Rees B, Thierry JC, Moras D. 1991. Class II aminoacyl transfer RNA synthetases: crystal structure of yeast aspartyl-tRNA synthetase complexed with $tRNA^{Asp}$. *Science* **252:** 1682–1689.

Saenger W. 1984. *Principles of nucleic acid structure*. Springer-Verlag, New York.

Samhita L, Shetty S, Varshney U. 2012. Unconventional initiator tRNAs sustain *Escherichia coli*. *Proc Natl Acad Sci* **109:** 13058–13063.

Samhita L, Nanjundiah V, Varshney U. 2014. How many initiator tRNA genes does *Escherichia coli* need? *J Bacteriol* **196:** 2607–2615.

Sarkhel S, Rich A, Egli M. 2003. Water-nucleobase "stacking": H-π and lone pair-π interactions in the atomic resolution crystal structure of an RNA pseudoknot. *J Am Chem Soc* **125:** 8998–8999.

Schmitt E, Panvert M, Blanquet S, Mechulam Y. 1998. Crystal structure of methionyl-$tRNA_f^{Met}$ transformylase complexed with the initiator formyl-methionyl-$tRNA_f^{Met}$. *EMBO J* **17:** 6819–6826.

Schmitt E, Panvert M, Lazennec-Schurdevin C, Coureux PD, Perez J, Thompson A, Mechulam Y. 2012. Structure of the ternary initiation complex aIF2-GDPNP-methionylated initiator tRNA. *Nat Struct Mol Biol* **19:** 450–454.

Schneider TD, Stephens RM. 1990. Sequence logos: a new way to display consensus sequences. *Nucleic Acids Res* **18:** 6097–6100.

Schrodinger, LLC. 2010. *The PyMOL Molecular Graphics System, Version 1.3r1*.

Schulman LH, Pelka H. 1975. The structural basis for the resistance of *Escherichia coli* formylmethionyl transfer ribonucleic acid to cleavage by *Escherichia coli* peptidyl transfer ribonucleic acid hydrolase. *J Biol Chem* **250:** 542–547.

Selmer M, Dunham CM, Murphy FV IV, Weixlbaumer A, Petry S, Kelley AC, Weir JR, Ramakrishnan V. 2006. Structure of the 70S ribosome complexed with mRNA and tRNA. *Science* **313:** 1935–1942.

Senecoff JF, Rossmeissl PJ, Cox MM. 1988. DNA recognition by the FLP recombinase of the yeast 2 μ plasmid. A mutational analysis of the FLP binding site. *J Mol Biol* **201:** 405–421.

Sham YY, Chu ZT, Warshel A. 1997. Consistent calculations of pKa's of ionizable residues in proteins: semi-microscopic and microscopic approaches. *J Phys Chem B* **101:** 4458–4472.

Shi H, Moore PB. 2000. The crystal structure of yeast phenylalanine tRNA at 1.93 Å resolution: a classic structure revisited. *RNA* **6:** 1091–1105.

Tao J, Perdew JP, Staroverov VN, Scuseria GE. 2003. Climbing the density functional ladder: nonempirical meta-generalized gradient approximation designed for molecules and solids. *Phys Rev Lett* **91:** 146401.

von Pawel-Rammingen U, Astrom S, Bystrom AS. 1992. Mutational analysis of conserved positions potentially important for initiator tRNA function in *Saccharomyces cerevisiae*. *Mol Cell Biol* **12:** 1432–1442.

Warshel A, Naray-Szabo G. 1997. *Computational approaches to biochemical reactivity*. Kluwer Academic Publishers, New York.

Weigend F, Ahlrichs R. 2005. Balanced basis sets of split valence, triple zeta valence and quadruple zeta valence quality for H to Rn: design and assessment of accuracy. *Phys Chem Chem Phys* **7:** 3297–3305.

Wilcox JL, Ahluwalia AK, Bevilacqua PC. 2011. Charged nucleobases and their potential for RNA catalysis. *Acc Chem Res* **44:** 1270–1279.

Yatime L, Schmitt E, Blanquet S, Mechulam Y. 2004. Functional molecular mapping of archaeal translation initiation factor 2. *J Biol Chem* **279:** 15984–15993.

Zhang J, Ferre-D'Amare AR. 2013. Co-crystal structure of a T-box riboswitch stem I domain in complex with its cognate tRNA. *Nature* **500:** 363–366.

Zhang J, Ferre-D'Amare AR. 2016. The tRNA elbow in structure, recognition and evolution. *Life* **6:** 3.

Zubay G. 1962. The isolation and fractionation of soluble ribonucleic acids. *J Mol Biol* **4:** 347–356.